Tight-binding Ising modeling of the interplay between bulk ordering and surface segregation in Pt-Ag nanoalloys

Abir Hizi, Alexis Front, Moncef Said, Fabienne Berthier, G. Tréglia, Christine Mottet

Tight-binding Ising modeling of the interplay between bulk ordering and surface segregation in Pt-Ag nanoalloys.

Abir Hizi[1,2], Alexis Front[2], Moncef Said[1], Fabienne Berthier[3], Guy Tréglia[2] and Christine Mottet[2] [a]

[1] *Laboratoire de la Matière condensée et Nanosciences, Faculté des Sciences de Monastir, Université de Monastir, Tunisie.*

[2] *Aix-Marseille Université, CNRS, CINaM UMR 7325, Campus de Luminy, 13288 Marseille, France. and*

[3] *Université Paris-Saclay, CNRS, Institut de chimie moléculaire et des matériaux dOrsay, 91405 Orsay, France.*

(Dated: May 12, 2020)

Abstract

We use a Tight-Binding Ising Model (TBIM) with effective pair interactions depending on concentration able to reproduce the bulk phase diagram of Pt-Ag system and in particular its strong asymmetry as a function of composition. This system presents both an $L1_1$ ordered structure around equiconcentration and a wide miscibility gap on the Pt-rich side. Using Monte Carlo simulations in canonical and semi-grand canonical ensembles, we succeed in reproducing qualitatively the bulk phase diagram and we study the equilibrium configurations of the (111) and (100) surfaces, and truncated octahedron clusters. The infinite surfaces reproduce sensibly the bulk phase diagram except that they present a strong silver surface segregation limited to the top surface layer. The clusters behave differently due to the reduction of the miscibility gap when decreasing the cluster size and present two typical ordered phases related to the $L1_1$ phase: one characterized by pure concentric atomic layers starting from silver surface layer which extends up to the center of the cluster, and the other one at higher silver concentration where the $L1_1$ phase is perfectly oriented along one (111) direction of the cluster. The later one has already been reported by recent experiments [1].

[a] corresponding author, e-mail: mottet@cinam.univ-mrs.fr

Keywords:

Alloys Surfaces; Nanoalloys; Surface segregation; chemical ordering; Monte Carlo simulations; Tight-Binding Ising model.

I. INTRODUCTION

Pt-Ag systems have been recently reinvestigated both in bulk alloys[2] and in nanoalloys[1, 3, 4] because of fundamental and applied interests. Pt-based alloys play an important role in catalytic applications[4–6] and notably in fuel cells[7–9] where it is necessary to decrease the amount of platinum in the cathodes to reduce the cost. From a fundamental point of view, Pt-Ag system displays a quite atypical phase diagram [2, 10, 11] with a large miscibility gap between two solid solutions at temperature between 1470 and 1170 K : one Pt-rich with a few percent of Ag up to 15% at 1470 K and the other Ag-rich with up to 40% at 1470 K. Below 1170 K there is an ordered stoechiometric compound, around the equiconcentration, precisely at $Ag_{47}Pt_{53}$. It is ordered according to the $L1_1$ structure which is an alternation of pure atomic layers in the (111) orientation (CuPt-type structure). First principles calculations of the Ag-Pt system coupled with a cluster variational method show that the cluster interactions have to be expanded beyond the second nearest neigbors in order to stabilize the miscibility gap between the two solid solutions at high temperature[11] and the $L1_1$ ordered structure as in the CuPt ordered compound[12]. The specifity of the Pt-Ag alloy is to display both phase separation and ordering tendency in the same system. This implies to use a theoretical model where the Effective Paire Interactions (EPIs) strongly depend on the concentration.

We use a quite simple theoretical model based on a Tight-Binding Ising Model (TBIM)[13] on a rigid lattice where the Effective Pair Interactions (EPIs) are fitted to *ab-initio*, semi-empirical Tight-Binding interatomic potential calculations or experimental data. We vary the EPIs as a function of the concentration in the alloy in order to take into account the specificity of the Pt-Ag system which presents both a miscibility gap and an ordered phase. Variation of the EPIs has already been used in Fe-Cr alloys to take into account short-range-order reversal as a function of concentration evidenced by diffuse-neutron-scattering and resistivity measurements [14]. Numerical simulations are performed using Monte Carlo

simulations in canonical and semi-grand canonical ensembles in order to describe systems at a given concentration (canonical) or at a given difference of chemical potential (semi-grand canonical) enabling to vary the concentration and temperature to describe phase diagrams. We also apply the Widom method in order to connect the two statistic ensembles.

The chemical ordering and surface segregation are crucial to control catalytic properties[4–9]. Nanoalloys represent systems of choice for catalytic applications since they optimize surface atoms as compared to the total weight of metal catalyst. However their structure and morphology vary sensibly as compared to bulk stucture [15–17]. Therefore a lot of studies are needed to characterize experimentally the nanoparticles and theoretically predict chemical arrangement notably at the surface where experimental results are still very scarce[1]. We use the semi-empirical SMA (Second Moment Approximation) potential developped for the Pt-Ag nanoalloys [1] and compared to *ab initio* calculations on small cluster sizes to fit a more simple energetic model on rigid lattice with variable EPIs as a function of the concentration. It is made to reproduce qualitatively the bulk phase diagram in the solid state part which means the $L1_1$ typical ordered phase and the phase separation between the two solid solutions at high temperature. Then we use it to characterize the surface segregation profile at the vicinity of the surface and we apply it to clusters of different sizes in the truncated octahedral shape.

The paper is divided in five parts including introduction and conclusion. The second part gives a description of the theoretical energetic model and atomistic simulations. The third and fourth parts describe the results respectively on the bulk and on the alloy surfaces and nanoalloys.

II. TIGHT-BINDING ISING MODEL AND MONTE CARLO SIMULATIONS

A. Concentration dependent Tight-Binding Ising Model

The Tight-Binding Ising Model (TBIM) [13, 18] has been developped to study chemical ordering effects in metallic alloys and surface segregation effects in semi-infinite [19] or finite systems [20, 21]. It is developped according to a Tight-Binding Hamiltonian, on a rigid lattice, where order/disorder phenomena are well treated. The rigid lattice assumption is partially compensated by adding a relaxation correction taking into account the lattice

misfit that we fit using a tight-binding second moment approximation (TB-SMA) interatomic potential. The hamiltonien writes in terms of effective pair interactions (EPI) V_{nm} between atoms at sites n and m, and occupation factors p_n with an Ising character which means $p_n = 1$ if the site n is occupied by an atom of type A or $p_n = 0$ if not (i.e. the site n is occupied by a B-type atom):

$$H^{TBIM} = \sum_{n,m} p_n p_m V_{nm} + \sum_n p_n (\Delta h_n^{coh} + \Delta h_n^{size}) \tag{1}$$

where the EPI $V_{nm} = \frac{1}{2}(V^{AA} + V^{BB} - 2V^{AB})$ characterizes chemical ordering. The second term corresponds to a local contribution to the energy induced by inequivalent geometrical environments in inhomogeneous systems like surfaces or clusters. It is composed of a cohesive term (Δh_n^{coh}) due to the cohesion difference of the two metals, and a relaxation term (Δh_n^{size}) due to size mismatch between the two elements, which is added to correct the rigid lattice assumption. They are nonzero for sites n which belong to the surface. Δh_n^{coh} is equal to the difference of surface energies of the two elements (promoting the element with the lowest one to segregate). They are calculated using the many-body SMA interatomic potential [1] on each different sites of a truncated octahedron cluster of 1289 atoms. We checked that the values obtained on the cluster facets are the same as the one obtained on infinite surfaces in order to use the same parameters for clusters and infinite surfaces. Δh_n^{size} are also calculated in the framework of the SMA potential by taking an impurity which differs from the matrix only by its atomic radius and corresponds to the difference in energy for a system with the impurity at the surface (infinite surface or cluster surface) as compared to the impurity in the bulk (or in the core of the cluster). The systems are quenched at 0 K by quenched molecular dynamic simulations. The values are listed in Tab. I.

The determination of the EPIs is more tricky. In the face centered cubic structure (fcc), it has been shown [22] that first neighbours interactions V_1 (for sites n and m first neighbours) dominate as compared to the following V_2, V_3, V_4. Therefore in general, we consider only first neighbours pairs V_1. However, at equiconcentration, to stabilize the $L1_1$ phase of the PtAg alloy with respect to the $L1_0$ or A_2B_2 ones, it is necessary to go at least to the second neighbours EPIs. The corresponding ground states on fcc lattice is shown on Fig. 1 [12, 23]. This phase diagram results from the description of each phase in terms of pair interactions. The stability domain for the $L1_1$ phase involves $V_2 > 0$ and $V_2 > V_1/2$ if $V_1 > 0$, or $V_2 > -V_1$

if $V_1 < 0$ (as illustrated by the diagram on Fig. 1). V_1 and V_2 EPIs can be fitted to the mixing enthalpies of the $L1_1$ and $L1_0$ phases calculated either by density functional theory (DFT) calculations or semi-empirical potentials.

The ab-initio calculations are performed within the density functional theory (DFT) and the generalized gradient approximation (GGA) using the Perdew and Wang [24] exchange and correlation functional and the projector augmented wave (PAW) [25, 26] interaction potential between the ions and the electrons, using the VASP code. The s and d valence electrons are considered for each metal with a cutoff energy equal to 600eV for plane wave basis set. The Brillouin zone integration is performed with the Monkhorst-Pack scheme with k-point mesh comprising 12 to 19 subdivisions along each reciprocal lattice vector. The cohesive energy and lattice parameter of pure Ag and Pt, and the formation energies of the $L1_1$ and $L1_0$ ordered phases have been optimized. The results are shown in Tab. II and compared to the same quantities obtained with the semi-empirical potential developped by Pirart *et al.* in ref. [1]. We check first that the formation energies of the alloy ordered phases calculated by DFT [11] are quite similar with the present ones. Our calculations are lower in energy but the difference between the two phases is comparable (90 to 100 meV). The large discrepancy comes from the TB-SMA calculations for which the formation energy of the $L1_1$ phase has been intentionally overestimated as compared to the $L1_0$ one in order to stabilize the $L1_1$ phase in bulk phase diagram [1, 27].

Beside the equiconcentration we need to describe all the concentration range between Pt-pure and Ag-pure systems. For that purpose we determine the EPIs by comparing energy of systems with impurity pair far separated versus neighboring. The energy difference between two impurities in first or second neighbors and the two impurities far away in the metal corresponds to V_1 or V_2 respectively. In Table III are listed the EPIs in bulk for the first (V_1) and second (V_2) neighbors in the two diluted limits and for the equiconcentrations as deduced from the formation energy of the ordered phase. We notice that they vary sensibly between the Pt-rich and the Ag-rich phases when calculated by TB-SMA whereas their variations are much smaller but still there in DFT, with a change of sign of V_1 in DFT as in TB-SMA and a positive value of V_2 in DFT even if much lower than in TB-SMA. As mentioned before, knowing that the formation energy of the $L1_1$ is overestimated in TB-SMA in order to stabilize the phase, this can explain the difference between DFT and TB-SMA calculations. In such a case we chose to fit the EPIs to the TB-SMA values. Then we take

into account their variations by fitting a polynomial function with the three EPIs values in order to use appropriate value according to the concentration in silver of the system leading to the concentration dependence illustrated in Fig. 2. We also checked that the EPIs values at equiconcentration respect the criteria to stabilize the $L1_1$ ordered phase.

The symmetry breaking at surfaces implies that the EPIs are modified at the surface [13, 28]. They have been determined by TB-SMA calculations in the same way as for the bulk but for sites located at the surface (the last atomic layer before the vacuum). We distinguish parallel interactions $V_i^{\parallel}$ where the two atoms are neigbouring in the surface layer, and perpendicular interactions $V_i^{\perp}$ for which the two atoms are neigbouring between two atomic layers perpendicularly to the surface. $V_i^{\parallel}$ is the energy difference between a slab where two impurities are located in-plane in first or second neighbour distance and a slab with the two impurities in-plane but far away one from the other. $V_i^{\perp}$ is the energy difference between a slab where two impurities are located out-of-plane with the same conditions. The values are reported in Tab. IV. We use a similar polynomial function as in the bulk to take into account their variations as a function of the concentration (see Fig. 2). Because we do not determined specific EPIs for the edge and vertex sites of the clusters, we take the same EPIs as the (100) surface sites. They appear in the following expression of the difference in energy between a surface site "p" and a bulk site for what concerns the alloying effect:

$$\Delta E_p^{alloy} = (Z_1 + 2Z_1')V_1 + (Z_2 + 2Z_2')V_2 - (Z_1 V_1^{\parallel} + Z_1' V_1^{\perp}) - (Z_2 V_2^{\parallel} + Z_2' V_2^{\perp}) \qquad (2)$$

where Z_1 and Z_2 are the first and second neighbors in the p plane and Z_1' and Z_2', the same out of plane.

It follows that the TBIM presents three phenomenological effects to control the surface segregation: the alloying effect which, at least in case of first neighbours interactions, favours the segregation of the minority element when $V < 0$, or the majority element with an oscillating profile when $V > 0$, but here with V_2 of the same order of V_1 this usual prediction does not strictly applied; the cohesive effect (Δh^{coh}) which promotes the segregation of the element with the lowest cohesive energy; and the size effect (Δh^{size}) which promotes the segregation of minority atom when it is the biggest one.

B. Monte Carlo simulations

We performed Monte Carlo simulations in canonical (N_{Ag}, N_{Pt}, P and T constant) and semi-grand canonical ensembles ($\Delta\mu = \mu_{Pt} - \mu_{Ag}$, N_{tot}=N_{Pt}+N_{Ag}, P and T constant) where atoms exchange (exchange the position of two atoms of different nature), respectively atoms permutations (permute the nature of one atom: A in B or B in A), are proposed and accepted according to a Metropolis sampling [29] insuring to reach a Boltzmann distribution of the chemical configurations at equilibrium. In canonical ensemble, the concentration remains constant whereas in the semi-grand canonical ensemble, the concentration varies and the difference of the chemical potential of the two elements remains constant. In each case we keep the same number of atoms in the simulation box.

To check the equivalence of the two statistical ensembles we can determine in canonical ensemble the chemical potential for a given concentration according to the Widom method [30]. We propose virtual permutations (Pt in Ag or Ag in Pt) to evaluate the averaged chemical potential at constant concentration, "virtual" because the system is unchanged as if there was no permutation. It is only made to evaluate the variation of the energy after the permutation and to deduce the chemical potential:

For a permutation of Pt in Ag:

$$\Delta\mu^{Pt->Ag} = \mu_{Ag} - \mu_{Pt} = -k_B T ln\{(\frac{1}{N_{Ag}+1})(\frac{M_{Ag}}{M_{Pt}}) \sum_{Pt\ atoms} e^{-\frac{\Delta E^{Pt->Ag}}{k_B T}}\} \quad (3)$$

and for a permutation of Ag in Pt:

$$\Delta\mu^{Ag->Pt} = \mu_{Pt} - \mu_{Ag} = -k_B T ln\{(\frac{1}{N_{Pt}+1})(\frac{M_{Pt}}{M_{Ag}}) \sum_{Ag\ atoms} e^{-\frac{\Delta E^{Ag->Pt}}{k_B T}}\} \quad (4)$$

where N_{Pt} and N_{Ag} are the total numbers of Pt and Ag atoms, M_{Ag}, M_{Pt} their masses and $\Delta E^{Pt->Ag}$ the variation in energy. In our model with rigid lattice the masses are not taken into account so that $\frac{M_{Ag}}{M_{Pt}} = 1$. Then we restore the system in its initial state and we proceed that way a large number of times (around 20000) to perform ensemble averages and get the equilibrium $\Delta\mu$ value. At equilibrium the $\Delta\mu^{Pt->Ag}$ and $\Delta\mu^{Ag->Pt}$ must be equivalent. This method has been used in different studies [31, 32] to connect the semi-grand canonical ensemble with the canonical ensemble.

For such simulations, we performed ten to twenty thousands macrosteps after leaving the system being equilibrated during two to five thousands macrosteps. Each macrostep

consists in proposing randomly to any atom of the box a chemical exchange (exchange or permutation). For bulk systems, periodic conditions are applied in each cristallographic direction whereas in surfaces they are applied only in two directions and for clusters there are no periodic conditions.

It is important to notice that the calculation of the energy difference between two configurations which comes into the exponential in the probabilities calculation, even if it concerns only two atoms over a few thousands, is very sensitive to the variation of the EPIs when they are not constant as in our present model. Therefore it is necessary to calculate at each step the total energy of the system instead of a partial one which concerns only a sphere of atoms located around the permuting or exchanged atoms, as it is usually done in Monte Carlo simulations to save computer time.

III. PT-AG BULK PHASE DIAGRAM

We first perform semi-grand canonical Monte Carlo simulations to determine isotherms along the whole composition range starting from Pt-pure system up to Ag-pure system or reversely. The curves in Fig. 3 show the equilibrated concentration when we vary the chemical potential difference $\Delta\mu$ up and down. We notice a large hysteresis between upward and downward curves in the semi-grand canonical ensemble for temperatures below 7000 K. The upward curve starts with a quasi Pt-pure phase which changes to an Ag-rich solid solution. The downward curve starts with the Ag-rich phase containing up to 60% of Pt (as compared to 40% in the upward curve) creating a large and asymmetric hysteresis between the two curves. The instability domain with two coexisting phases increases when the temperature decreases. We use the Widom method in canonical ensemble to better characterize the transition and determine the exact critical concentrations in order to plot the phase diagram. First we notice that outside the phase coexisting domain the curves obtained within the two ensembles are fully superimposed which confirms that the statistical calculations are well converged. Inside the phase coexisting domain, the canonical ensemble explores instable states whereas semi-grand canonical ensemble explores both stable and metastable states. To extract the stable states and define the domain limits of each phase we determine the critical chemical potential in the canonical curve with the "s" curve. The critical concentrations are deduced from the s-curve (shown in red in Fig. 3) where we divide

the area on both side of the "s" in two equal parts as illustrated by the Figure 4. After defining the critical $\Delta\mu$ it is easy to extract the corresponding concentrations in Pt-rich (c_1) and Ag-rich (c_2) phases that will be reported on the bulk phase diagram. We get a very asymmetric miscibility gap with a quasi Pt-pure phase (c_1 around zero) and a solid solution where Ag is majoritary, which is a result of the variation of the EPIs as a fonction of the concentration.

When increasing the temperature up to 7000 K (Fig. 3) we notice that the semi-grand canonical Monte Carlo curve becomes continuous, similar to the canonical curve and the hysteresis disappears. Above 7000 K the phase diagram displays a solid solution along the whole composition range.

At low temperature, below 2000 K, the chemical structure becomes ordered according to the $L1_1$ phase around the equiconcentration as shown in Fig. 5. This phase is characterized by the sublattices occupation illustrated on Fig 5 where on each consecutive (111) layer the sublattices are occupied alternatively by Ag and Pt atoms. To characterize the order/disorder transition we performed canonical simulations at constant concentration and for increasing or decreasing temperatures. Due to the strong asymmetry of the Pt-Ag system, the $L1_1$ phase is not centered on the equiatomic composition but rather at 60% of silver which characterizes the critical order/disorder temperature equal to 2200 K. To characterize the concentration domain of the $L1_1$ phase we performed Widom canonical simulations where the permutations are virtual but we explore all the composition range at constant temperature. In Fig. 6 we show the variation of the global Ag composition as a function of the chemical potential together with the four sublattices occupations. The s-curve of the canonical Widom simulation illustrates the phase coexistence between the quasi-pure Pt phase with c_1 almost equal to zero and the ordered $L1_1$ phase at c_1' around 0.5. This limit is obtained by the same rule as performed at high temperature via the critical chemical potential corresponding to the separation of the instable domain in two equal areas. With the corresponding sublattices occupation (equally occupied two by two) we can characterize the $L1_1$ phase in coexistence with the Pt-rich solid solution. The second limit of the $L1_1$ phase domain is not characterized by an "s" loop on the canonical curve which means this second transition is continuous going progressively from a very strongly overstoechiometric $L1_1$ phase (near 75% of silver) to a Ag-rich disordered solid solution. The limit is then characterized by the separation of the four sublattices equally occupied two by two in the

grand canonical simulations.

In the experimental phase diagram [2, 10, 11] the ordered $L1_1$ phase transforms into a coexistence domain between two solid solutions at 1200 K. Our model reproduces the miscibility gap but at a higher temperature (2100 K) than the experimental one (Fig. 7). Our model has also the tendency to underestimate the solubility limit in the Pt-rich domain and to overestimate the solubility limit in the Ag-rich domain. Finally the domain of the $L1_1$ ordered phase is much more broaden in our model. Nevertheless, using a quite simple model, we get a qualitatively satisfying bulk phase diagram for solid phases as compared to the experimental one, with notably a nice anisotropy thanks to the variations of the EPIs.

IV. (111) AND (100) PT-AG ALLOYS SURFACES

Because of the very large difference between the cohesive energy of the two elements (see Table I), we expect to get a quite substantial silver surface segregation on the Pt-Ag alloys surfaces in order to minimize the total energy of the system. We will see in the following how the surface segregation influences the chemical configuration at the vicinity of the two most compact surfaces: (111) and (100). Depending on the temperature, we will also study how the surface segregation takes place with the different chemical ordering tendencies present in the bulk phase diagram i.e. phase separation between 2000 K and 7000 K and ordering with the $L1_1$ phase below 2000 K.

The Monte Carlo simulations in the semi-grand canonical ensemble are performed at different temperatures on slabs constituted by 40 atomic layers with about one hundred of atoms each (exactly 100 atoms for the (111) orientation and 72 atoms for the (100) one). We checked that the results we show are independent of the size of the slab as soon as the thickness of the slab is sufficiently large (more than 30 atomic layers) in order to get the bulk conditions in the middle of the slab.

We will consider in the next sections the (111) and (100) infinite surfaces at high temperature (above the ordering temperature for the $L1_1$ phase) and at room temperature.

A. (111) and (100) Pt-Ag surfaces at high temperature

The infinite (111) and (100) surfaces present a strong silver surface segregation for each temperature up to 7000K where the system becomes fully disordered in the bulk. At lower temperatures (5000K or 3000K) there is a miscibility gap between the two solid solutions as in the bulk phase diagram. The segregation isotherms are illustrated on Fig. 8 for the (111) and (100) surfaces. We observe a slight oscillation profile in the (111) surface because of the alternation of (111) atomic layers that recalls the $L1_1$ ordered phase even for temperatures higher than the order/disorder transition. This is a signature of the ordering tendency of the Pt-Ag system which is consistent with the (111) surface orientation and not with the (100) where only the top surface layer in enriched with silver, then very slightly the second one.

We could have expected a more important segregation for the (100) orientation as compared to the (111) one because of the effect of the broken bonds, the more open the surface the more important the segregation. This was not the case for a similar system, the Cu-Pt alloys [19], where a very unusual anisotropy was found: in that case, the Cu surface enrichment was stronger for the close-packed (111) surface than for the more open (100) one, contrary to usual arguments based on the anisotropy of surface energy. In Pt-Ag, at high temperature, the surface anisotropy is negligeable. We will see in the following by comparing cluster facets that a slight anisotropy exists and the segregation is slightly stronger on the (111) facets as compared to the (100) ones, in agreement with the results reported on Cu-Pt system [19].

B. (111) Pt-Ag surface at 300 K

The (111) Pt-Ag surface at room temperature is made of a silver pure atomic surface layer, for any composition larger than a limit concentration of Ag which is linked to the thickness of the slab. It corresponds to a system with a quasi Pt pure bulk (core of the slab) and two Ag surface layers on each side (the slab presenting two surfaces). This limit concentration $c^*_{Ag} = 2/n_p$, where n_p is the number of atomic layers in the slab, tends naturally to zero for an infinite number of layers. Typically, in the results presented on Fig. 9, $c^*_{Ag} = 0.05$ for a slab made of 40 atomic layers. Beyond c^*_{Ag}, the system presents a miscibility gap or phase

coexistence between a quasi Pt-pure bulk with only the top surface layer Ag-pure, and the $L1_1$ phase. The stable domain of this ordered phase starts at equiconcentration up to 80% of Ag. By increasing the Ag concentration, the core of the slab is made of the Ag-rich solid solution with still the Ag pure surface layer. As in the bulk, there is a large miscibility gap between the quasi Pt-pure solid solution and the $L1_1$ ordered phase. The $L1_1$ ordered phase starts to nucleate near the surface because of the presence of the Ag surface segregation by a continuation of the alternate staking of Ag and Pt pure layers.

C. (100) Pt-Ag surface at 300 K

At low silver concentration, before the filling of the whole surface as in the (111) orientation, the (100) Pt-Ag surface starts with a surface superstructure with silver atomic rows in the $< 110 >$ direction leading to the (1x2) surface structure (see Fig. 10-(a)). Then we get the pure Ag surface layer on top of the Pt quasi-pure phase (Fig. 10-(b)), as in the (111) surface, and just after, a second pure Ag sub-surface layer (Fig. 10-(c)). The miscibility gap represents a coexistence of two phases: the purely segregated configuration and the Ag segregated one with the $L1_1$ ordered phase beneath. This structure is displayed on Fig. 10-(d). The up and down curves are not fully superimposed because of the phase coexistence: the structure Fig. 10-(c) appears in the "up" simulation only and the structure Fig. 10-(d) only in the down simulation. Also in the down curve we notice a continuous variation of the concentration of the sub-surface layer (c_1) up to the mixte composition of the plane. This composition of 50% corresponds to the (2x1) ordering which forms the $L1_1$ ordered phase according to the (100) orientation. As for the (111) surface, the miscibility gap is delimited by the Ag surface segregation limit on the left and the occurence of the $L1_1$ phase on the right. This domain is nicely comparable to the one of the bulk phase diagram (Fig. 7).

To conclude for the infinite surfaces compared to bulk phase diagram, the infinite systems behave essentially as the bulk except that a part of the phase separation concerns the Ag surface segregation. In the next section, concerning alloys clusters, we will see the effect of the finite size of the system, particularly the finite reservoir of silver matter and the morphology of the cluster, on the chemical arrangement of the nanoalloys.

V. PT-AG ALLOYS CLUSTERS

We study truncated octahedron (TOh) clusters of 1289 and 2951 atoms with both (111) and (100) facets and compare the segregations on these facets to the surface segregation of related infinite surfaces. We also study the behaviour of the miscibility gap for the finite size cluster system as compared to the other infinite systems (bulk and surfaces).

TOh are made of (111) and (100) facets connected by edges and vertices at the surface and we will consider all the other sites as core sites. We perfomed semi-grand canonical Monte Carlo simulations as in the infinite surfaces at different temperatures.

A. Pt-Ag nanoalloys at high temperature

In the Figure 11 we have reported the segregation isotherms of the 1289-atoms TOh cluster at high temperatures as for the (111) and (100) surfaces (Fig. 8). By comparison of the cluster facets with the corresponding infinite surface, we notice that the surface segregation (c_0 in Fig. 8) is the same as the cluster facet ones ((111) and (100) facets in Fig. 11) on the condition of considering the segregation isotherms plotted as a function of the core concentration (c_{core}) (right column of Fig. 11). The finite matter effect (limited quantity of Ag) in clusters is remarkable when the site concentrations are plotted as a function of the global concentration since all the silver atoms segregate to the surface, the core remaining Pt-pure up to a global concentration of 40% of Ag (of course depending on the cluster size). First the vertex, then the edge sites are occupied by Ag atoms, followed closely by the (100) and (111) facets sites. The hierarchy of occupation of the different types of surface sites on the cluster follows the broken bonds except for the facets since the (111) facets are slightly more enriched in Ag than the (100) ones. This is counter intuitive because it does not follows the hierarchie of broken bonds. However a similar reversal of segregation concerning the (100) and (111) facets had been observed in Cu-Ag clusters [20] rather due to a coupling between the edges with the facets. Here there can be two effects: the inversion can be intrinsec to the system because as in the Cu-Pt system [19], the chemical ordering with positive V_2 can influence the segregation differently and in small clusters there can be some influence of the edges. Anyway the anisotropy is rather weak.

When all the surface sites are occupied by Ag atoms, which represents around 40 % of

the total number of sites in the TOh_{1289} cluster, then the core of the cluster begins to be populated by Ag atoms, forming a disordered solid solution because of the high temperature (higher than the critical order/disorder temperature).

Finally, one notices the absence of miscibility gap in the cluster below 7000 K, at the difference with the bulk phase diagram (Fig. 7) or the infinite surfaces (Fig. 8).

B. Pt-Ag nanoalloys at 500 K

By decreasing the temperature below 2000 K, we get the $L1_1$ ordered phase around 70 % of silver in the cluster, which is clearly characterized by the sublattice occupation illustrated in the bottom graph of Fig. 12 and Fig. 12-(c). Just before the complete ordering of the core with the four sublattices two-by-two occupied, we notice that the four sublattices are not fully randomly distributed but two over the four are partially ordered i.e. one is enriched in Ag, the other is pure in Pt. Clearly the definition of these sublattices is not appropriate to characterize a new ordering but looking at the chemical arrangement in Fig. 12-(b) we observe that the structure is made of concentric atomic layers alternatively occupied by Ag and Pt atoms. Everything happens as if one $L1_1$ ordered phase nucleates beneath all the (111) facets. This structure is effectively stabilized in our model in a composition range between 60 and 70 % of silver. Then one perfect $L1_1$ domain occupies all the cluster core focusing on one (111) facet orientation. This is in agreement with the experimental and modelisation with interatomic SMA potential of small Pt-Ag nanoclusters [1]. However, the SMA potential predicted the formation of at most three alternated concentric atomic layers in the vicinity of the surface. Such interatomic potential allows atomic relaxations which is not the case in our TBIM rigid model. Within SMA potential, the subsurface Pt segregation forming the first concentric layer below the surface is due to the lattice mismach between Ag and Pt and to the inward surface relaxation of the cluster surface, inducing a subsurface stress in compression which can be released by putting smaller atoms below the surface. In the present study, because of the rigid lattice assumption, we cannot get surface relaxation effects leading to specific subsurface segregation. However we demonstrate here that the chemical EPIs interactions lead to the formation of these two kinds of ordering depending on the concentration, one with concentric pure atomic layers alternating Ag and Pt, the other with the $L1_1$ ordered phase along one of the (111) orientation of the clusters,

as illustrated on Fig. 12.

We also notice that the hierarchy of segregation of the different sites of the cluster respect the same as at high temperature (see Fig. 11, and the shifts are even enhanced by lowering the temperature. This leads to a structure where all the verteces and edges are occupied by Ag atoms whereas the facets are rather rich in Pt before 20 % of silver in the cluster and between 30 and 40 % of silver, only the (111) facets are populated by Ag whereas the (100) have around 30 % of Ag atoms. However we must recall that the (100) facets contain only 9 sites, so that 30 % of Ag atoms corresponds to the (2x1)(100) surface reconstruction.

Finally we show the finite size and matter effect on the width of the miscibility gap in the clusters of 1289 and 2951 atoms (Fig. 13). The larger the size of the cluster, the wider the miscibility gap between the core-shell structure and the ordered one starting with the concentric alternated layers. This confirms that by increasing the size, the cluster should behave like the bulk phase diagram. Moreover, in the clusters, at the difference with the infinite surfaces, we notice another miscibility gap between the first surface site occupation up to 0.05 % of Ag and the almost complete core-shell structure. This means that the core-shell structure driven by the strong Ag surface segregation is too much concentrated in silver to be compatible with the Pt-rich solid solution so that there are some forbidden phases around 20 % of silver in the cluster. These are very new and surprising results which show the specificities of the nanoalloys as compared to systems with infinite reservoirs.

VI. CONCLUSIONS

Using a quite simple Tight-Binding Ising model, on rigid lattice, with variable EPIs as a function of the concentration, we successfully reproduce the asymmetric and original bulk phase diagram of the Pt-Ag system where both separated and ordered phase are present depending on temperature and concentration. We applied our model to (111) and (100) surfaces and truncated octahedron clusters of 1289 and 2951 atoms. All the systems show a strong silver surface segregation and then a chemical ordering according to the $L1_1$ bulk ordered phase. In the (111) surface, this structure is just the surface termination of the alternate staking of Ag pure, Pt pure layers. In the (100) case, after the filling of the first surface layer with silver atoms, the $L1_1$ phase grows in the second and following alternate staking of Pt and Ag atomic planes along the (111) direction. In the clusters case, the surface

segregation of one atomic plane corresponds to a core-shell structure whereas the chemically ordered $L1_1$ phase appears in two different ways: at lower silver concentration, the $L1_1$ ordering appears below each (111) oriented facets leading to a pure onion-shell structure alternating Ag pure and Pt pure concentric layers; at higher concentration, we observe a single oriented $L1_1$ phase with a silver pure surface shell as in the experiments [1]. We also analyzed the evolution of the miscibility gap domains in the clusters, as compared to the surfaces and bulk and show the effect of finite size and finite matter on the phase diagrams of nanoalloys. Such study is a step towards the characterization of nanoalloys phase diagrams. A simple model as the TBIM is further promising in order to study kinetics and aging of nanoalloys.

ACKNOWLEDGMENTS

This work was granted access to the HPC resources of IDRIS under the allocation 2017-096829 made by GENCI. The authors would like also to acknowledge support from the International Research Network - IRN "Nanoalloys" of CNRS.

[1] J. Pirart, A. Front, D. Rapetti, C. Andreazza-Vignolle, P. Andreazza, C. Mottet, and R. Ferrando, Nat. Comm. **10**, 1982 (2019).

[2] G. Hart, L. Nelson, R. Vanfleet, B. Campbell, M. Sluiter, J. Neethling, E. Olivier, S. Allies, C. Lang, B. Meredig, and C. Wolverton, Acta Materialia **124**, 325 (2017).

[3] J. Wisniewska, H. Guesmi, M. Ziolek, and F. Tielens, J. Alloys and Compounds **770**, 934 (2019).

[4] J. Wisniewska, C.-M. Yang, and M. Ziolek, Catalysis Today **333**, 89 (2019).

[5] Y. Pan, I. Yan, Y. Shao, J.-M. Zuo, and H. Yang, Nano Lett. **16**, 7988 (2016).

[6] S. Hwang, C. Zhang, E. Yurchekfrodl, and Z. Peng, J. Phys. Chem. C **118**, 28739 (2014).

[7] J. Xu, T. Zhao, and Z. Liang, J. Phys. Chem. C **112**, 17362 (2008).

[8] A. Esfandiari, M. Kazemeini, and D. Bastani, Int. J. Hydrog. Energy **41**, 20720 (2016).

[9] J. Cao, M. Guo, J. Wu, J. Xu, W. Wang, and Z. Chen, J. Power Sources **277**, 155 (2015).

[10] P. Durussel and P.Feschotte, Journal of Alloys and Compounds **239**, 226 (1996).

[11] M. Sluiter, C. Colinet, and A. Pasturel, Phys. Rev. B **73**, 174204 (2006).

[12] A. Senhaji, G. Tréglia, and B. Legrand, Surface Science **307-309**, 440 (1994).

[13] G. Tréglia, B. Legrand, and F. Ducastelle, Europhys. Lett. **7**, 575 (1988).

[14] I. Mirebeau and G. Parette, Phys. Rev. B **82**, 104203 (2010).

[15] R. Johnston and R. Ferrando, eds., *Nanoalloys: From Theory to Application*, Faraday Discuss., Vol. 138 (RSC Publishing, 2008).

[16] R. Ferrando, J. Jellinek, and R. Johnston, Chem. Rev. **108**, 845 (2008).

[17] D. Alloyeau, C. Mottet, and C. Ricolleau, eds., *Nanoalloys, Synthesis, Structure and Properties*, Engineering Materials (Springer-Verlag, London, 2012).

[18] G. Tréglia, B. Legrand, F. Ducastelle, A. Saúl, C. Gallis, I. Meunier, C. Mottet, and A. Senhaji, Comp. Mater. Sci. **15**, 196 (1999).

[19] A. Khoutami, B. Legrand, and G. Tréglia, Surf. Sci. **287**, 851 (1993).

[20] F. Lequien, J. Creuze, and F. Berthier, J. Chem. Phys. **125**, 094707 (2006).

[21] F. Lequien, J. Creuze, F. Berthier, I. Braems, and B. Legrand, Phys. Rev. B **78**, 075414 (2008).

[22] A. Bieber, Thesis, Louis Pasteur University, Strasbourg (1987).

[23] F. Ducastelle, in *Order and Phase Stability in Alloys*, Cohesion and Structure, edited by F. R. de Boer and D. G. Pettifor (North-Holland, Elsevier Science Publishers B.V., Amsterdam, Oxford, New York, Tokyo, 1991).

[24] J. P. Perdew and Y. Wang, Phys. Rev. B **45**, 13244 (1992).

[25] P. E. Blöchl, Phys. Rev. B **50**, 17953 (1994).

[26] G. Kresse and D. Joubert, Phys. Rev. B **59**, 1758 (1999).

[27] A. Front, PhD thesis, Aix-Marseille University (2018).

[28] H. Dreyssé, L. T. Wille, and D. de Fontaine, Phys. Rev. B **47**, 62 (1993).

[29] N. Metropolis, A. Metropolis, M. Rosenbluth, A. Teller, and E. Teller, J. Chem. Phys. **21**, 1087 (1953).

[30] B. Widom, J. Chem. Phys. **39**, 2808 (1963).

[31] C. Varvenne, PhD thesis, Paris VI University (2010).

[32] M. Briki, PhD thesis, Paris-Sud University (2013).

(eV/at.)	Vertex	Edge	(100)	(111)
γ_n^{Pt}	0.60	0.50	0.67	0.51
γ_n^{Ag}	1.06	0.86	0.38	0.3
Δh_n^{coh}	-0.44	-0.36	-0.29	-0.21
Δh_n^{size}	Vertex	Edge	(100)	(111)
Pt(Ag)	-0.10	-0.12	-0.13	-0.10
Ag(Pt)	-0.002	0.008	0.02	0.01

TABLE I. TBIM on site parameters related to surface segregation driving forces: cohesion effect Δh_n^{coh} which is the difference in surface site energies(γ_n^{Metal}) between Pt and Ag metals, n being either a site of cluster surface (facets) or infinite surfaces, and size effect Δh_n^{size} which is the difference in energy of one impurity at surface site n as compared to the same impurity in the bulk, the impurity being distinct of the matrix only by its atomic radius (see text). Calculations are performed with the tight binding TB-SMA interatomic potential.

	a($\AA$)	E_{coh} (eV/at)	ΔH_{L1_1}	ΔH_{L1_0}
Ag				
DFT-GGA	4.16	-2.725		
TB-SMA	4.16	-2.725		
Exp.	4.09	-2.950		
Pt				
DFT-GGA	3.98	-5.53		
TB-SMA	3.98	-5.53		
Exp.	3.92	-5.86		
AgPt				
DFT-GGA			-0.051	0.041
DFT-GGA [11]			-0.039	0.063
TB-SMA			-0.213	0.063

TABLE II. DFT (GGA) and semi-empirical (TB-SMA) calculations of the formation enthalpies (in eV/at.) of the AgPt ordered phases compared to other DFT calculations [11] and experimental data (Kittel, Wiley, New York, 1996). The formaton enthalpies of the ordered ($L1_1$ and $L1_0$) phases are defined as the energy difference between the ordered system and the demixed one without interface which means pure Pt and pure Ag metals. The TB-SMA potential has been fitted to reproduce the DFT values of the lattice parameter and cohesion energy of the pure metals [1].

EPI (eV/at.)	Pt(Ag)	PtAg	Ag(Pt)
V_1			
DFT-GGA	-0.012	-0.013	0.007
TB-SMA	-0.086	-0.016	0.002
V_2			
DFT-GGA	0.034	0.027	0.001
TB-SMA	0.007	0.087	0.106

TABLE III. Effective pair interactions (EPI) extended to first V_1 and second V_2 neighbors for different concentrations: impurity of Ag in Pt "Pt(Ag)" and impurity of Pt in Ag "Ag(Pt)" in the bulk calculated by DFT (GGA) and semi-empirial (TB-SMA).

(eV/at.)	$V_1^{\parallel(111)}$	$V_1^{\perp(111)}$	$V_2^{\perp(111)}$	$V_1^{\parallel(100)}$	$V_2^{\parallel(100)}$	$V_1^{\perp(100)}$	$V_2^{\perp(100)}$
Pt(Ag)	-0.026	-0.081	0.062	-0.048	0.032	-0.112	0.045
Ag(Pt)	0.002	0.003	0.115	0.075	0.115	0.002	0.100

TABLE IV. Effective pair interactions (EPIs) at the (111) and (100) surfaces calculated with TB-SMA potential.

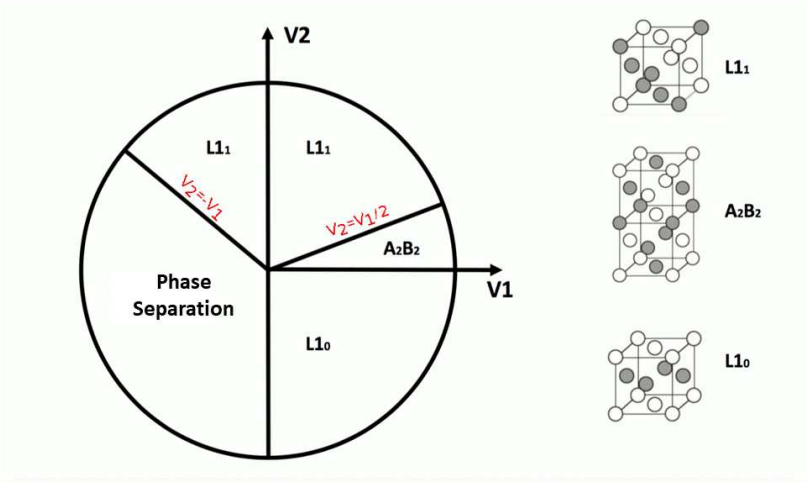

FIG. 1. Ground state diagram of an Ising model for Effective Pair Interactions (EPIs) on fcc lattice at first and second neighbors [12, 23, 27].

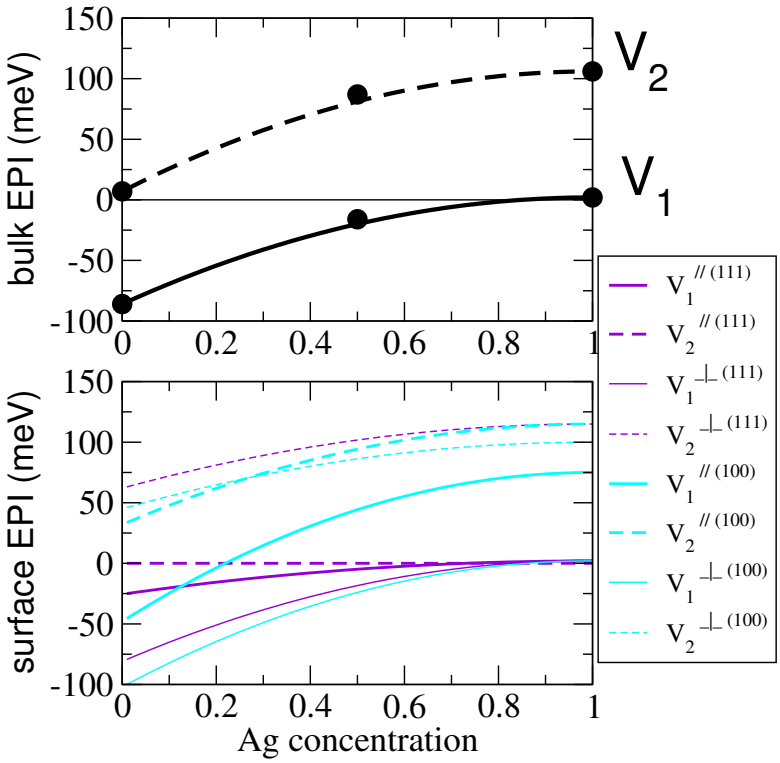

FIG. 2. Effective pair interactions (EPIs) at first and second neighbors as a function of the silver concentration in bulk (top graph) and at (111) and (100) surfaces (bottom graph).

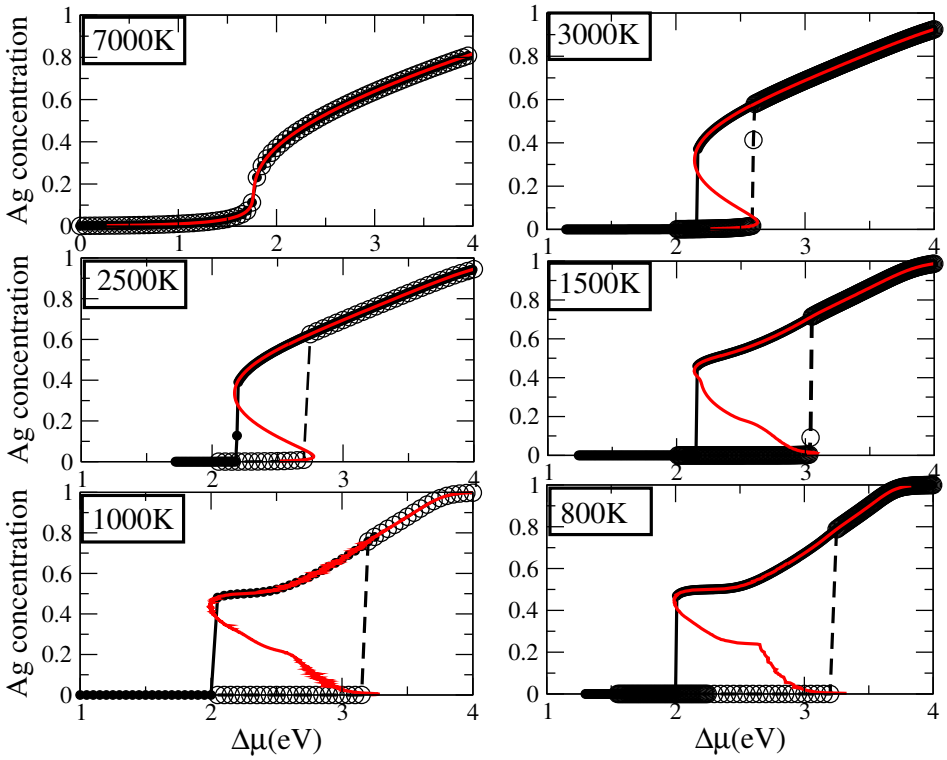

FIG. 3. Bulk isotherms determined via semi-grand canonical Monte Carlo simulations with increasing (dashed line) and decreasing (straight line) $\Delta\mu$ from pure Pt metal (on the left) to pure Ag metal (on the right) or via canonical Monte Carlo simulation using the Widom method (virtual permutations) (red line).

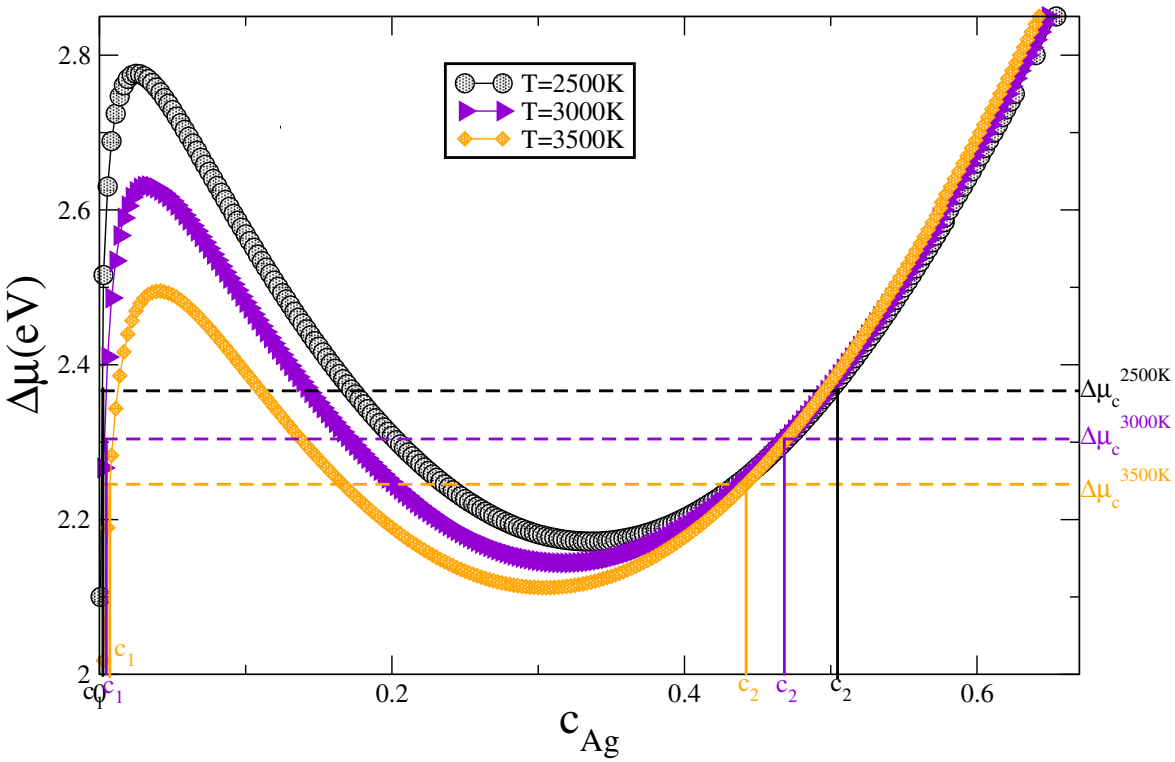

FIG. 4. Characterization of the critical concentrations c_1 and c_2 at high temperature from the canonical Monte Carlo simulations using virtual permutations.

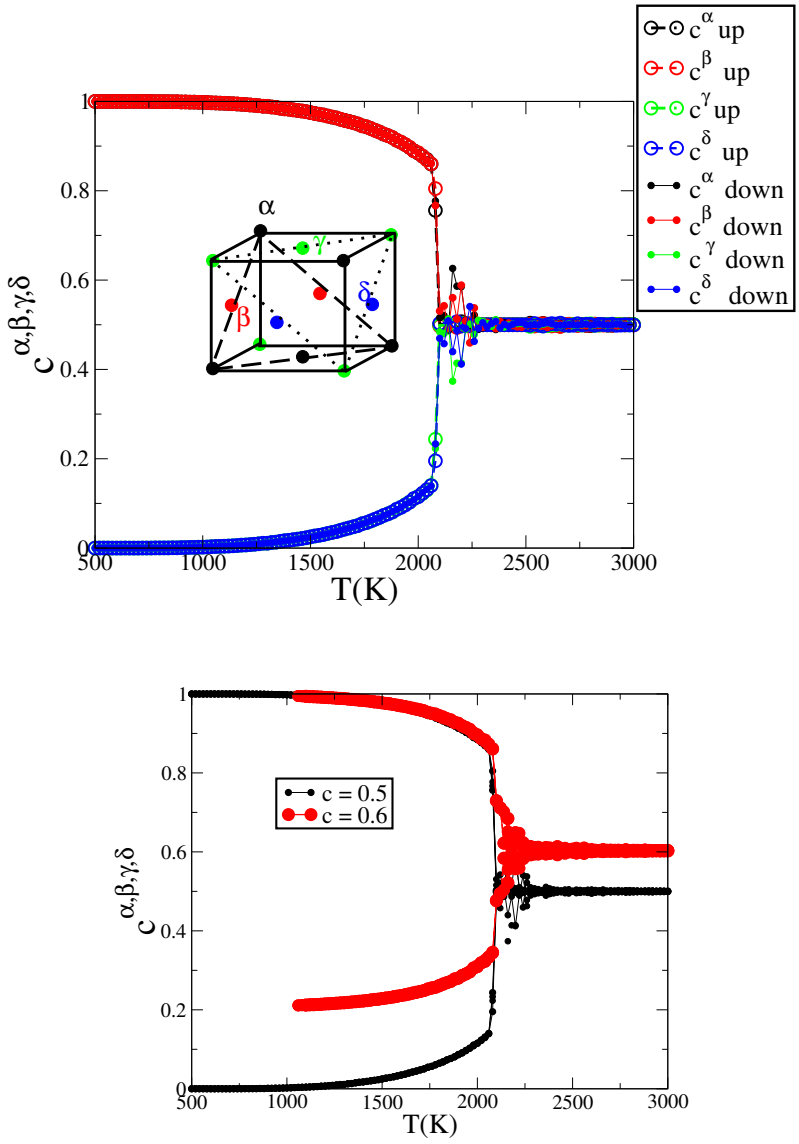

FIG. 5. Bulk sublattices from canonical Monte Carlo simulations at equiconcentration (top graph) and c=0.6 (bottom graph) with increasing (up) and decreasing (down) temperature. The sublattices are defined relatively to the (111) cristallographic planes. The $L1_1$ phase is characterized by the sublattices occupied two by two by Ag or Pt atoms. The disordered A1 solid solution is characterized by the four sublattices equally occupied.

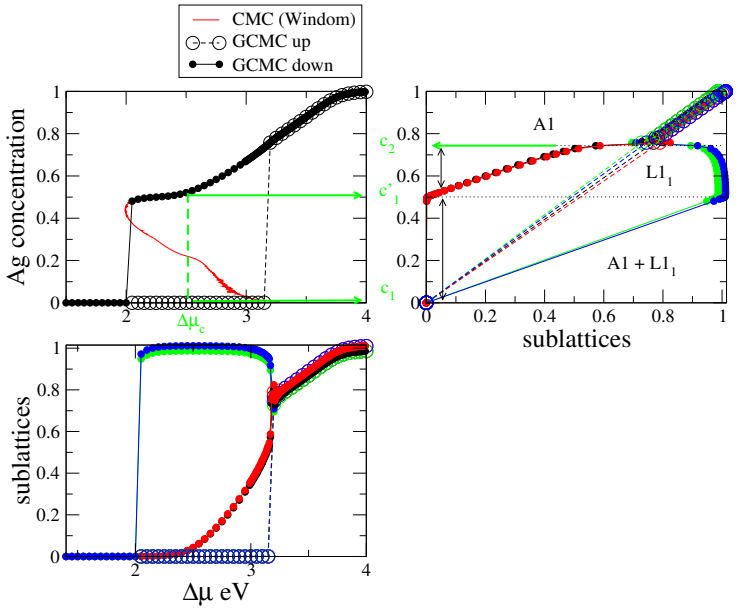

FIG. 6. Top left, the global Ag concentration as a function of the chemical potential at 1000 K from semi-grand canonical Monte Carlo (in black) and canonical Widom Monte Carlo simulations with virtual permutations (in red) as in Fig. 3. The corresponding sublattices occupations plotted as a function of the chemical potential $\Delta\mu$ (bottom left) and as a function of the global Ag concentration (top right). The critical $\Delta\mu$ which separates the "s" loop in two equal areas allows to characterize the concentration c_1' limiting the phase coexistence domain (instability domain in canonical simulation) and the pure $L1_1$ phase characterized by the sublattices equally occupied two by two. The c_2 between the $L1_1$ and the Ag-rich solid solution is deduced from the grand canonical curves (GCMC down) whit the separation of the sublattices occupation two by two as compared to the equal occupation for the Ag-rich solid solution.

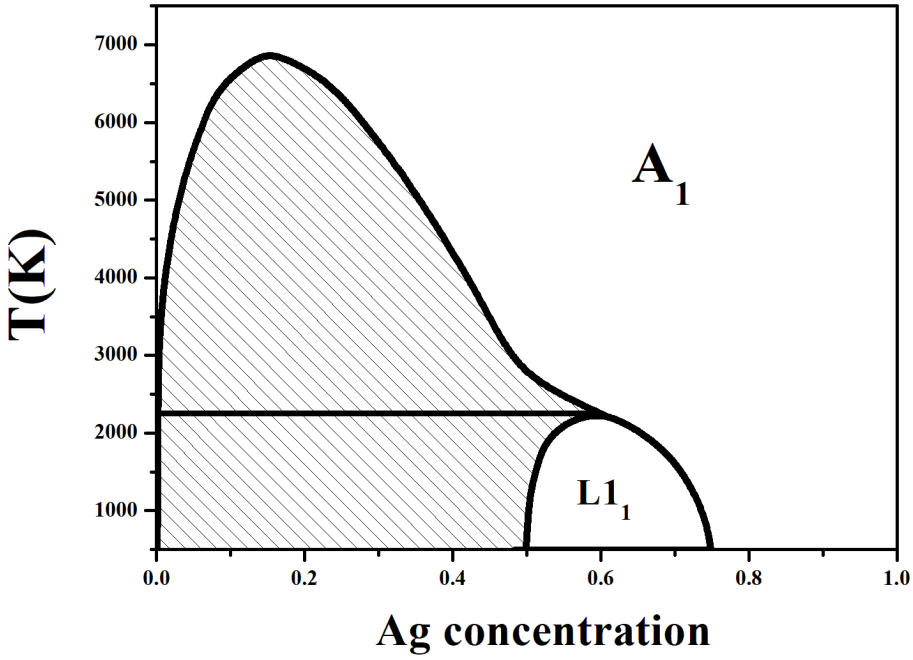

FIG. 7. Theoretical bulk phase diagram with the TBIM model and variable EPIs.

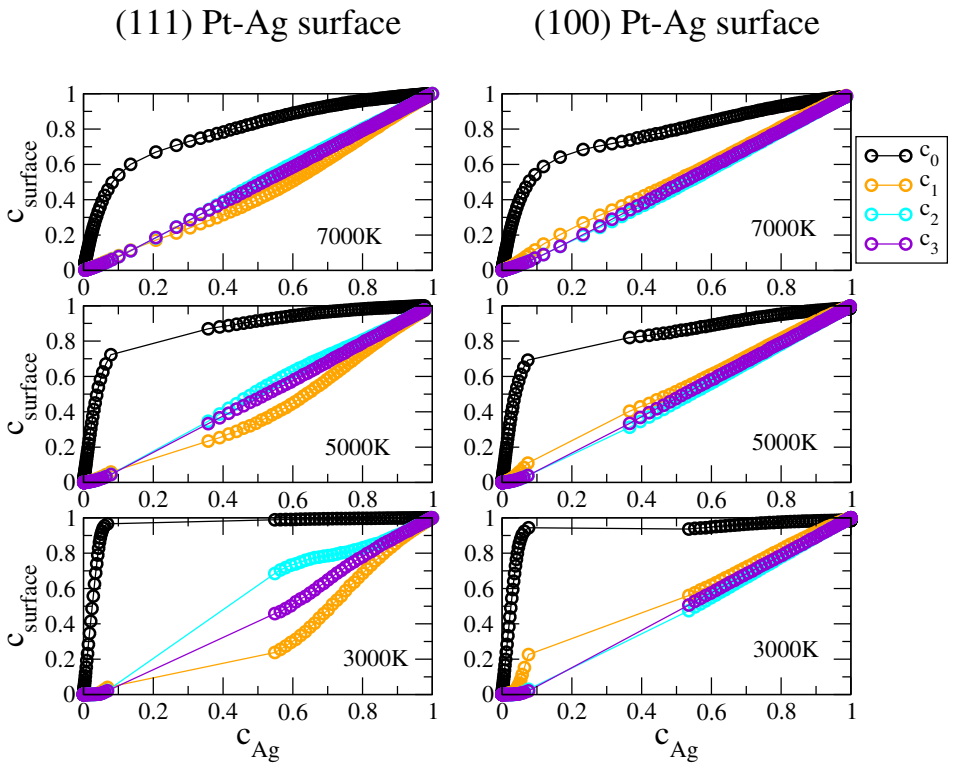

FIG. 8. Segregation isotherms at (111) and (100) surfaces at 7000K, 5000K and 3000K where we plot the top surface c_0, the subsurface c_1 and the following c_2 and c_3 atomic layers concentrations in silver by increasing (up) or decreasing (down) the chemical potential.

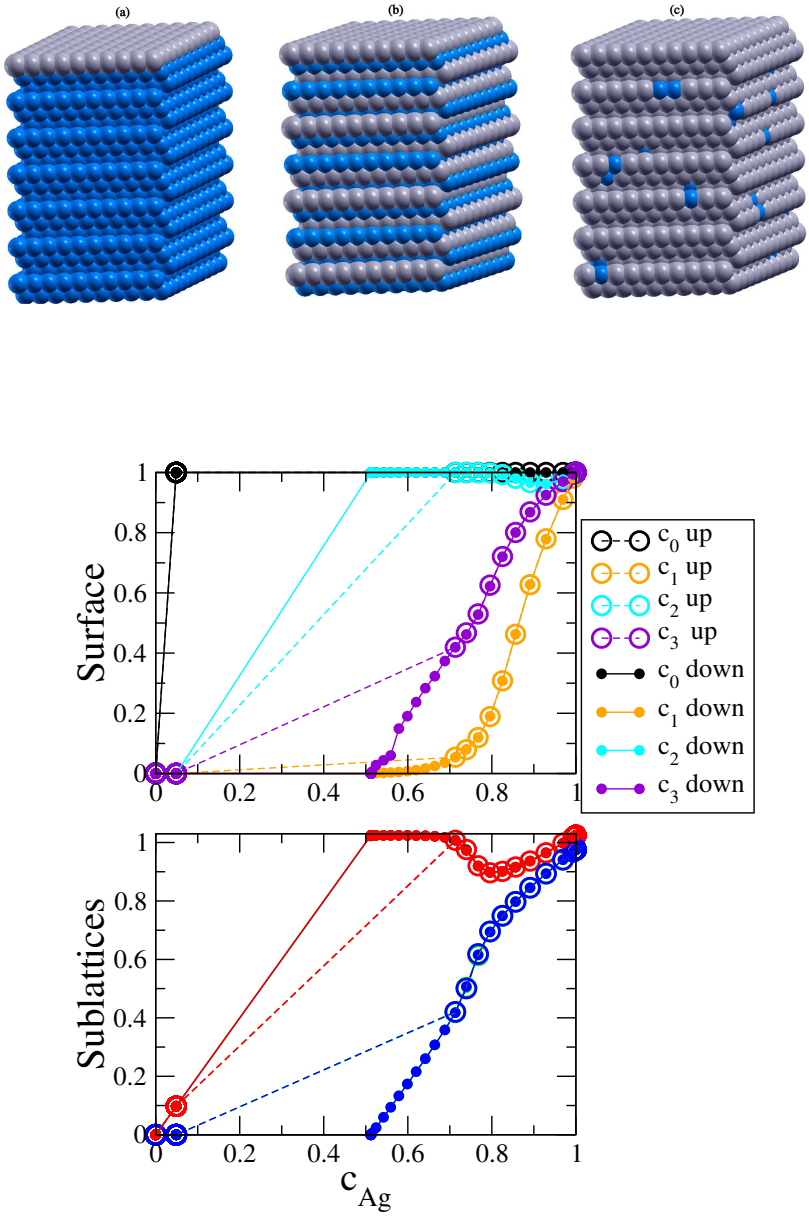

FIG. 9. Segregation isotherms of the (111) surface at 300 K. The slabs are illustrated on top for three characteristic concentrations (a) below 5%, (b) 50% and (c) above 80% with Ag atoms in grey and Pt atoms in blue. Then the first four layers concentrations starting from the surface c_0, c_1, c_2 and c_3 are plotted in the top graph and finally the core sublattices concentrations are plotted in the bottom graph as a function of the global Ag concentration.

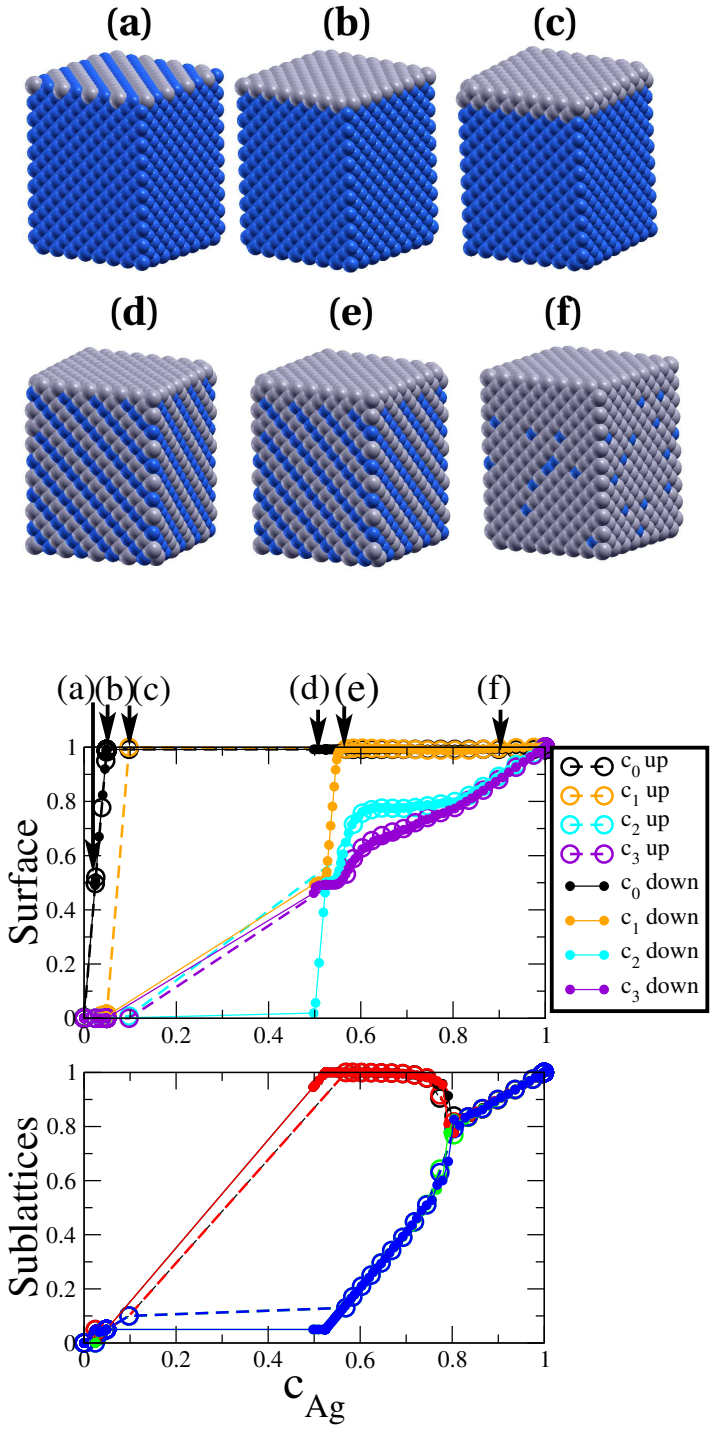

FIG. 10. Segregation isotherms of (100) surface at 300 K. The same as Fig. 9 with (a) for a concentration of 2.5%, (b) 5%, (c) 10%, (d) 50%, (e) 55% and (f) 90%.

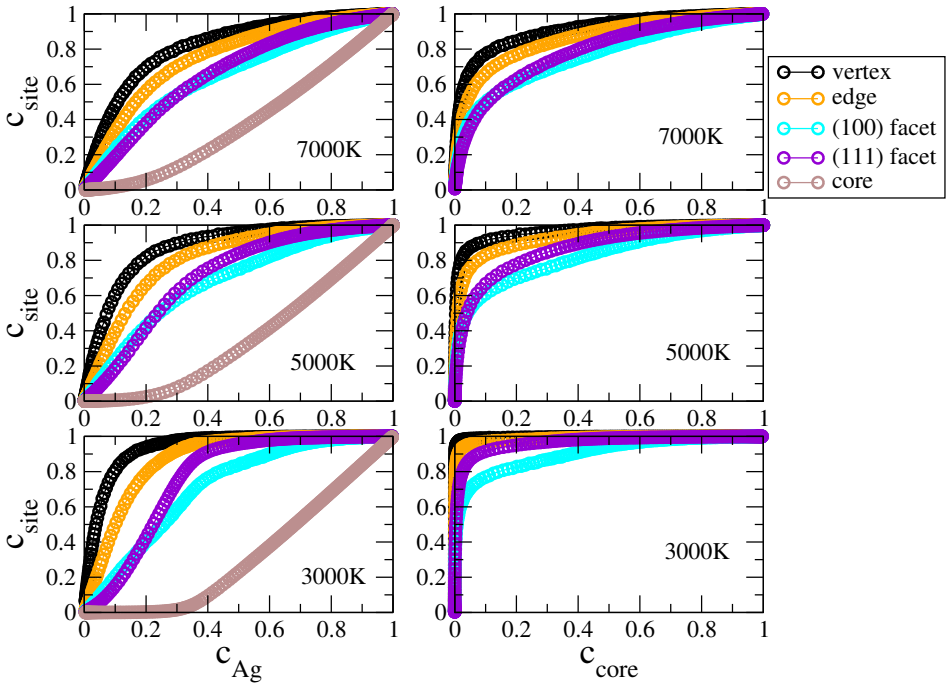

FIG. 11. Segregation isotherms of TOh_{1289} cluster at high temperature for each different surface sites (vertex, edge, (111) and (100) facets) and core sites, and for up and down simulations (which are superimposed) with the same symbols as for the surfaces. In the first line the site concentrations are plotted as a function of the global silver concentration (c_{Ag}) and in the second line the same site concentration are plotted as a function of the core concentration in silver (c_{core}).

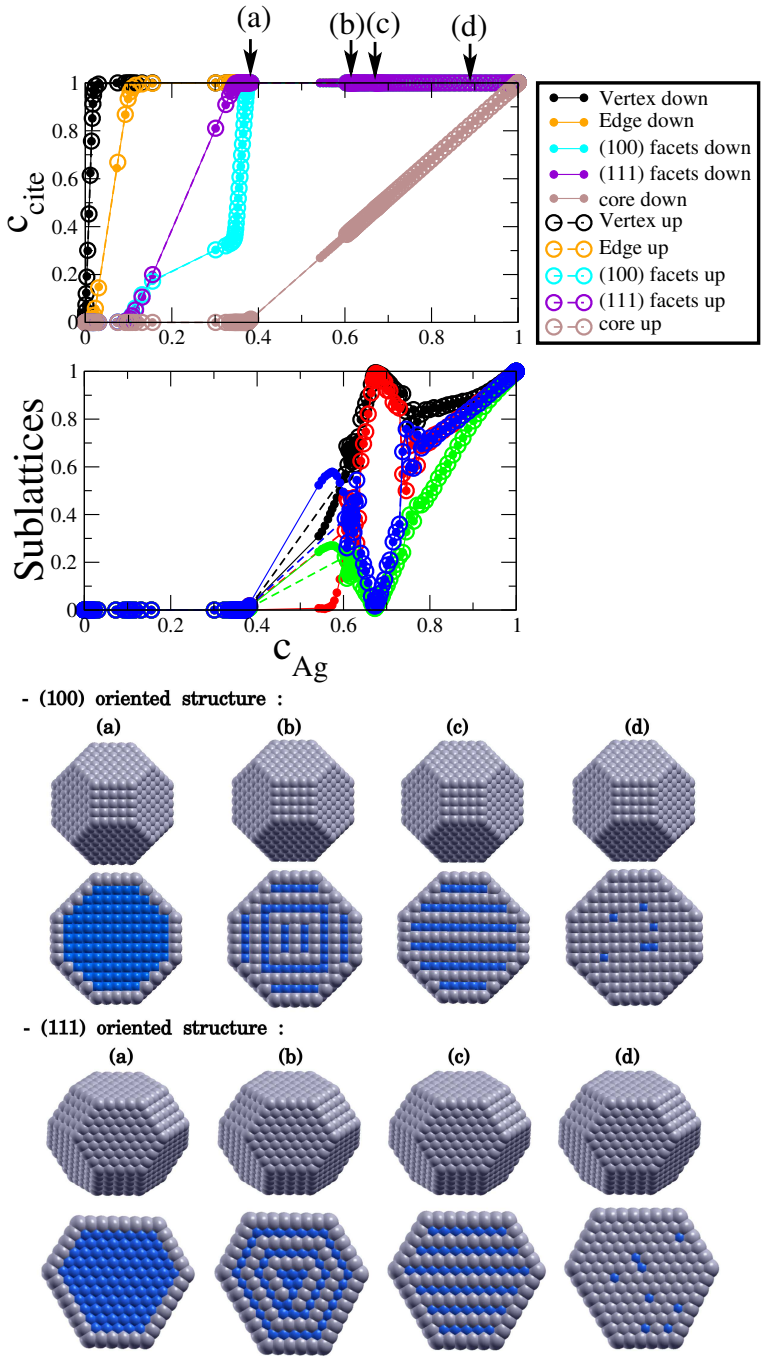

FIG. 12. Segregation isotherms of TOh_{1289} cluster at 500 K with the same legends as in Fig. 11 and the associated structures.

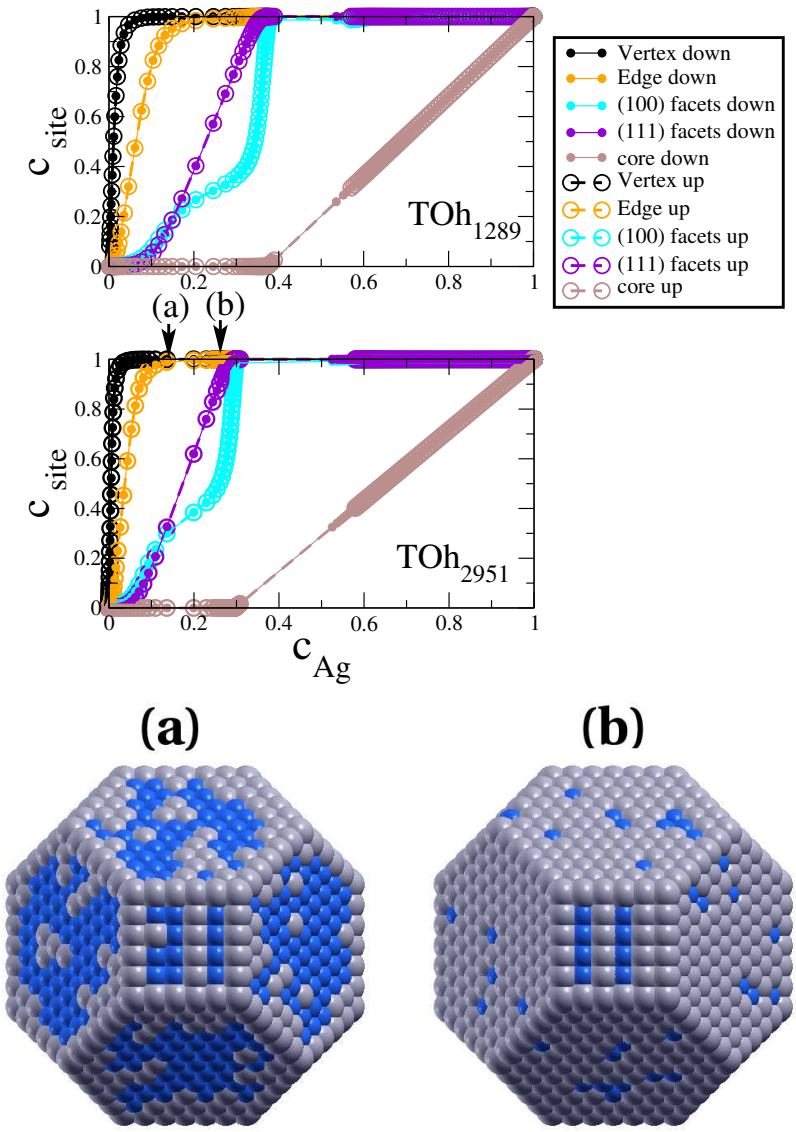

FIG. 13. Segregation isotherms of TOh_{1289} and TOh_{2951} cluster at 1000 K for each different surface sites (vertex, edge, (111) and (100) facets) and core sites, and for up and down simulations (which are superimposed) with the same symbols as for the surfaces. Illustration of the TOh_{2951} cluster at 5% (a) and 25% (b) of Ag.